 CMC, vol.4, no.2, pp.75-85, 2006

An Analytical Model for Shot-Peening Induced Residual Stresses

Shengping Shen[1], **S. N. Atluri** [2]

Abstract: To improve the fatigue life of metallic components, especially in aerospace industry, shot peening is widely used. There is a demand for the advancement of numerical algorithms and methodologies for the estimation of residual stresses due to shot peening. This paper describes an analytical model to simulate the shot peening process and to estimate the residual stress field in the surface layer. In this reasonable, convenient, and simple model, no empirical relation is used, and the effects of shot velocity are included. The results of validation of this model against the test data are very good.

keyword: Shot-peening, Residual Stress, Analytical Model

1 Introduction

Shot-peening is a cold-working process primarily used to extend the fatigue life of metallic structural components. Small spherical particles, typically made of metal with a high hardness, are made to impact the surface of the structural component at a velocity of 40-70 m/s. The shot peening process consists of multiple repeated impacts of a structural component by these hard spheres. Resulting from each impact, the structural component undergoes local plastic deformation. The elastic sub-surface layers should theoretically recover to their original shape during unloading, however continuity conditions between the elastic and the plastic zones do not allow for this to occur. Consequently, a compressive residual stress field is developed in the near-surface layer of the structural component. Since, fatigue cracks generally propagate from the surface of structural components, the resulting surface compressive residual stress field is highly effective in improving the early fatigue behavior of metals. The compressive residual stress field can significantly decrease the crack growth rate of short surface-cracks; therefore inherently causing the fatigue life extension of shot peened structural components.

Substantial experimental studies regarding residual stress distributions, and the influence of the processing parameters in relation to shot peening effectiveness has been conducted. And while, computer simulations of the shot peening process have also begun to receive attention in scientific literature, a comprehensive review of the current status of analytical and/or numerical approaches to the modeling of the shot-peening process reveals that the general field of shot peening is insufficiently developed. Further advancements in analytical/numerical algorithms and methodologies for the estimation of residual stresses due to shot-peening are clearly warranted.

The shot peening process is considerably complex: the system is dynamic, and includes contact. Despite the complicated nature of the problem, there were attempts to determine the residual stress field using approximate approaches and closed form solutions [Khabou, et al. (1990); Li, et al. (1991)]. Application of the Hertzian contact theory and an approximate elastic-plastic analysis for the surface-layer, allows for the estimation of the distribution of the compressive residual stress field due to shot peening. It is however, difficult to find the appropriate boundary conditions for the solution of quasi-static problem. One approach to overcoming this difficulty is to perform shot peening with a low coverage of the material surface, and then to estimate the force for the contact problem by measuring the size of shot dents [Khabou, et al. (1990)]. It was determined [Khabou, et al. (1990)] that it is more difficult to obtain good results for aluminum alloys because they show a complex hardening evolution.

Hertz's and Davis' contact theory furnishes the only relevant analytical solution: the static contact of a rigid sphere on an elastic semi-infinite space [Davis (1948); Johnson (1985)]. Residual stress distributions with better precision can be obtained with the use of numerical methods and computer simulation of the whole shot peening process. The finite element method is the most

[1] MOE Key Laboratory for Strength and Vibration, School of Aerospace, Xi'an Jiaotong University, Xi'an, Shaanxi 710049, P.R. China

[2] Center for Aerospace Research & Education, 5251 California Avenue, #140, University of California, Irvine, Irvine, CA 92617

suitable modeling method because of its reliability, and the possibility to implement complex material constitutive models. Some recent publications [Schiffner, et al. (1999); Deslaef, wt al. (2000); Meguid, et al. (1999)] show the potential of the finite element method for shot peening simulation. Many authors have proposed numerical solutions for the contact between a single sphere and an elasto-plastic half space, in the static and dynamic cases (a review can be found in [Al-Hassani (1981)] and [Zarka, et al. (1990)]). Meguid et al. (1999) presented a detailed analysis of two indentations on a semi-infinite medium, under dynamic conditions. Very few studies present the analysis of shot peening modeled by multiple indentations.

The whole shot peening simulation can be performed during one finite element dynamic elastic-plastic analysis. However, such an approach appears to be computationally inefficient. Typically the shot peening simulation is divided into two steps. The first step is a dynamic analysis of the shot-workpiece contact, which is aimed at the determination of boundary conditions for the second elastic-plastic step. The second step is a quasi-static elastic-plastic analysis, which produces the distribution of residual stresses. The dynamic contact problem for one shot is solved as an axisymmetric one by Schiffner et al. (1999). Displacements at the contact surface are used as boundary conditions for three-dimensional elastic-plastic multi-shot problem. A similar approach to the shot peening modeling is included in reference [Deslaef, wt al. (2000)]. Numerical analyses have been performed using the finite element package ABAQUS. The effect of shot velocity, size and shape on the residual stresses of a target exhibiting bilinear material behavior is examined in References [Meguid et al. (1999)]. The three-dimensional dynamic elastic-plastic analysis is performed using the finite element code ANSYS. Dynamic single and twin elastic-plastic spherical indentations were examined using rigid spherical shots and metallic targets. The results reveal that near-surface residual stresses are significantly influenced by the shot velocity, shot shape and separation distance between the co-indenting shots and to a much lesser extent by the strain-hardening rate of the target

Based on an elastic-perfectly plastic body, Al-Hassani (1981, 1982, 1984) developed an analysis model to predict residual stresses, which depend on the experimental results (there exist empirical relations to fit experimental results) to obtain certain critical relations. Guechichi et al. (1986) proposed a very complex model for elastic-plastic body. Li et al. (1991) developed a simplified analytical model for elastic-plastic body by regarding the shot peening process as a quasi-static case, which cannot take the velocity of the shot into account; and in addition, depends on empirical parameters to develop a theoretical model. In this paper, a new theoretical model is developed based on the initial models of Al-Hassani (1984) and Li et al. (1991) for modeling the shot-peening process and estimating the residual stress field in the surface layer. Principal developments are made to take the primary shot peening factors into consideration: characteristics of the material, diameter and velocity of the shot.

2 Fundamental equations for the elastic loading process

In this paper, it is assumed that the shot peened part (target material) is a semi-finite body. A homogeneous residual stress field and associated plastic strain exist at any specified depth due to the assumption that a semi-finite body has been uniformly loaded. To describe the maximum elastic loading, the impact of an elastic sphere on the surface of an elastic semi-finite body is analyzed. This can be considered as a particular application of Hertzian contact theory of between two elastic spheres.

According to the Hertzian contact theory, when the elastic compression is at its maximum, the radius of the elastic contact circle between the shot and the semi-finite body, is expressed as

$$a_e = R\left[\frac{5}{2}\pi k\rho\frac{V^2}{E_0}\right]^{\frac{1}{5}} \tag{1}$$

and the maximum normal elastic pressure is given by

$$p = \frac{1}{\pi}\left[\frac{5}{2}\pi k\rho V^2 E_0^4\right]^{\frac{1}{5}} \tag{2}$$

These two equations were initially proposed in Davies' work (1948) on dynamic elastic contact between a half-space and a ball of radius R, with:

$$\frac{1}{E_0} = \frac{1-v^2}{E} + \frac{1-v_s^2}{E_s} \tag{3}$$

where V is the initial velocity of the shot, p is the maximum normal pressure, R is the radius of the shot, and a_e

is at maximum the radius of the elastic contact circle, E and v, E_s and v_s, are Young's modulus and Poisson's ratio of the target and shot, respectively. k is an efficiency coefficient that stands for the thermal and elastic dissipation during the impact. The value of k is fixed at 0.8 according to Johnson (1985). A 100% k value will describe purely elastic rebound energy.

The classical Hertz results are used to model the elastic stress field created by the impact. The Hertzian elastic stress tensor can be written as follows:

$$\mathbf{T}^e = \begin{bmatrix} \sigma^e_{11} & 0 & 0 \\ 0 & \sigma^e_{22} & 0 \\ 0 & 0 & \sigma^e_{33} \end{bmatrix}$$

where the subscripts 1, 2, and 3 represents the axis x_1, x_2 and x_3, respectively. The axis x_3 directs along the depth of the target, and goes away from its surface. The elastic stress field is then obtained from the Hertzian theory. The stresses in the target material reach their maximum under the shot and can be written as

$$\begin{aligned} \sigma^e_{11} &= p\,(1+\nu)\left[\frac{x_3}{a_e}\tan^{-1}\left(\frac{x_3}{a_e}\right)-1\right]+p\frac{a_e^2}{2\left(a_e^2+x_3^2\right)} \\ \sigma^e_{22} &= p\,(1+\nu)\left[\frac{x_3}{a_e}\tan^{-1}\left(\frac{x_3}{a_e}\right)-1\right]+p\frac{a_e^2}{2\left(a_e^2+x_3^2\right)} \end{aligned} \tag{4}$$

$$\sigma^e_{33} = -p\left[1+\left(\frac{x_3}{a_e}\right)^2\right]^{-1} \tag{5}$$

According to the Hook's law, the strains are expressed as

$$\begin{aligned} \varepsilon^e_{11} &= \tfrac{1}{E}\left[\sigma^e_{11}-v\left(\sigma^e_{22}+\sigma^e_{33}\right)\right] \\ \varepsilon^e_{22} &= \tfrac{1}{E}\left[\sigma^e_{11}-v\left(\sigma^e_{22}+\sigma^e_{33}\right)\right] \end{aligned} \tag{6}$$

$$\varepsilon^e_{33} = \frac{1}{E}\left[\sigma^e_{33}-2v\sigma^e_{11}\right] \tag{7}$$

Thus, we can obtain the Von Mises equivalent stress in the target material as

$$\sigma^e_i = \left[\left(\sigma^e_{11}-\sigma^e_{22}\right)^2+\left(\sigma^e_{22}-\sigma^e_{33}\right)^2+\left(\sigma^e_{33}-\sigma^e_{11}\right)^2\right]^{\frac{1}{2}} \Big/ \sqrt{2} \tag{8}$$

Then, the equivalent strain can be obtained through the Hook's law as

$$\varepsilon^e_i = \frac{\sigma^e_i}{E} \tag{9}$$

And the mean stress and strain can be written as

$$\begin{aligned} \sigma^e_m &= \tfrac{1}{3}\left(\sigma^e_{11}+\sigma^e_{22}+\sigma^e_{33}\right) \\ \varepsilon^e_m &= \tfrac{1}{3}\left(\varepsilon^e_{11}+\varepsilon^e_{22}+\varepsilon^e_{33}\right) \end{aligned} \tag{10}$$

Now, the stress deviators in the target material can be derived as

$$\begin{aligned} s^e_{11} &= \sigma^e_{11}-\sigma^e_m = \tfrac{1}{3}\sigma^e_i \\ s^e_{22} &= \sigma^e_{22}-\sigma^e_m = \tfrac{1}{3}\sigma^e_i \end{aligned} \tag{11}$$

$$s^e_{33} = \sigma^e_{33}-\sigma^e_m = -\frac{2}{3}\sigma^e_i = -2s^e_{11} \tag{12}$$

Similar to the stress deviators, the strain deviators are derived as

$$\begin{aligned} e^e_{11} &= \varepsilon^e_{11}-\varepsilon^e_m = \tfrac{1}{3}(1+v)\,\varepsilon^e_i \\ e^e_{22} &= \varepsilon^e_{22}-\varepsilon^e_m = \tfrac{1}{3}(1+v)\,\varepsilon^e_i \end{aligned} \tag{13}$$

$$e^e_{33} = \varepsilon^e_{33}-\varepsilon^e_m = -\frac{2}{3}(1+v)\,\varepsilon^e_i = -2e^e_{11} \tag{14}$$

Now, the stress and strain tensors in the elastic field are derived. The elastic-plastic analysis of the loading process will be discussed in the subsequent section.

3 Elastic-plastic analysis of the loading process

The elastic-plastic regime presents a difficult theoretical problem that is still a subject of serious research effort. In the elastic-plastic deformation stage, the equivalent stress in the target material is greater than the yield stress, i.e., $\sigma_i > \sigma_s$; the stress-strain analysis becomes too complicated and inconvenient to apply in practice. It is very difficulty to directly use the complex elastic-plastic constitutive relation in engineering. It is however, worth resorting to a simple analytical treatment. As in many elastic-plastic analyses, the elastic-plastic constitutive relationship associated with the target material can be simplified to a multi-linear one. A simplified relation [Li, et al. (1991)] will be implemented here. By adopting a modifying coefficient, α, the elastic-plastic strain ε^p_i at any depth x_3 is calculated from the elastic strain ε^e_i, at the corresponding depth x_3:

$$\varepsilon^p_i = \begin{cases} \varepsilon^e_i \text{ for } \varepsilon^e_i \le \varepsilon_s \\ \varepsilon_s + \alpha\left(\varepsilon^e_i-\varepsilon_s\right) \text{ for } \varepsilon^e_i > \varepsilon_s \end{cases} \tag{15}$$

where ε_i^p and ε_i^e are functions of x_3 only, ε_s is the strain corresponding to the yield stress σ_s, and α is the ratio of plastic to elastic deformation and is defined as

$$\alpha = \frac{a_p}{a_e} \tag{16}$$

where a_e is given in equation (1), and a_p is the radius of a dent produced by the same shot on an elastic-plastic target under the same velocity. It is assumed that the ratio of ε_i^p to ε_i^e on the x_3-axis inside the target is equal to the ratio α of the deformation at the surface.

The derivation of the plastic radius a_p is begins with the equation of motion during contact:

$$\frac{4\pi}{3}\rho R^3 \frac{dV}{dt} = -\pi a^2 \overline{p} \tag{17}$$

As in reference [Al-Hassani (1984)], the stress field surrounding the indentation is assumed to be the same as for a pressurized spherical cavity in an elastic-plastic material. The cavity expands to accommodate the material displaced by the indenter. The model gives an approximate value for the average pressure $\overline{p}$ resisting the motion [Al-Hassani (1984)], as:

$$\frac{\overline{p}}{\sigma_s} = 0.6 + \frac{2}{3}\ln\frac{Ea}{\sigma_s R} \tag{18}$$

It then follows that:

$$\frac{\overline{z}}{R} = \left(\frac{2}{3}\right)^{\frac{1}{2}} \left(\frac{\rho V^2}{\overline{p}}\right)^{\frac{1}{2}} Q(\overline{z}) \tag{19}$$

Where,

$$1/Q = \left[\left(0.2 + \frac{2}{9}\ln\frac{E}{\sigma_s}\right) + \frac{1}{9}\left(\ln\frac{2\overline{z}}{R} - \frac{4\overline{z}}{R}\right)\right]^{\frac{1}{2}}$$

and $\overline{z}$is the final indentation [Al-Hassani (1984)]. This equation governs the initial stages of deformation but as soon as the pressure $\overline{p}$ reaches $3\sigma_s$ a rigid plastic analysis will hold. This may be found theoretically and has also received considerable experimental confirmation. By assuming pressure $\overline{p}$ to remain constant during the indentation process, the expression (19) will become

$$\frac{\overline{z}}{R} = \left(\frac{2}{3}\right)^{\frac{1}{2}} \left(\frac{\rho V^2}{\overline{p}}\right)^{\frac{1}{2}}$$

By means of

$$a^2 = 2\overline{z}R - \overline{z}^2 \tag{20}$$

A nonlinear equation of a is now formed, and the plastic radius $a_p$can be obtained by solving this nonlinear equation. These equations are derived for elastic-perfect plastic materials, but we still use them to approximate the plastic radius a_p for strain-hardened materials.

According to the elastic-plastic stress-strain curve (multilinear), the elastic-plastic stress σ_i^p is calculated as

$$\sigma_i^p = \begin{cases} \sigma_i^e \text{ for } \varepsilon_i^p < \varepsilon_s \\ \sigma_s + E_1\left(\varepsilon_i^p - \varepsilon_s\right) \text{ for } \varepsilon_s \le \varepsilon_i^p < \varepsilon_b \\ \sigma_b \text{ for } \varepsilon_i^p \ge \varepsilon_b \end{cases} \tag{21}$$

The definitions of the parameters are shown in Fig. 1, and σ_b is the ultimate tension strength.

To obtain the stress deviators, we should derive the strain deviators first. Due to the fact that the relationship between the strain deviators and ε_i^e, as in equations (13) and (14) for the elastic stage results from the axisymmetry of loading and geometric conditions, the corresponding relationship in the elastic-plastic stage will be kept to be same. Hence, the elastic-plastic strain deviators can be expressed as

$$\begin{aligned} e_{11}^p &= \tfrac{1}{3}(1+\nu)\varepsilon_i^p \\ e_{22}^p &= \tfrac{1}{3}(1+\nu)\varepsilon_i^p \end{aligned} \tag{22}$$

$$e_{33}^p = -\frac{2}{3}(1+\nu)\varepsilon_i^p = -2e_{11}^p \tag{23}$$

By appealing to the elastic-plastic theory, the elastic-plastic stress deviators can be derived from the following relationship

$$s_{ij}^p = \frac{1}{1+\nu}\frac{\sigma_i^p}{\varepsilon_i^p} e_{ij}^p \tag{24}$$

Thus, the elastic-plastic stress deviators can be obtained as

$$\begin{aligned} s_{11}^p &= \tfrac{1}{1+\nu}\tfrac{\sigma_i^p}{\varepsilon_i^p} e_{11}^p = \tfrac{1}{3}\sigma_i^p \\ s_{22}^p &= \tfrac{1}{1+\nu}\tfrac{\sigma_i^p}{\varepsilon_i^p} e_{22}^p = \tfrac{1}{3}\sigma_i^p \end{aligned} \tag{25}$$

$$s_{33}^p = -\frac{2}{3}\sigma_i^p = -2s_{11}^p \tag{26}$$

After the stress and strain tensors in the elastic-plastic field are obtained, we will derive an expression for the residual stress field after unloading, in the next section.

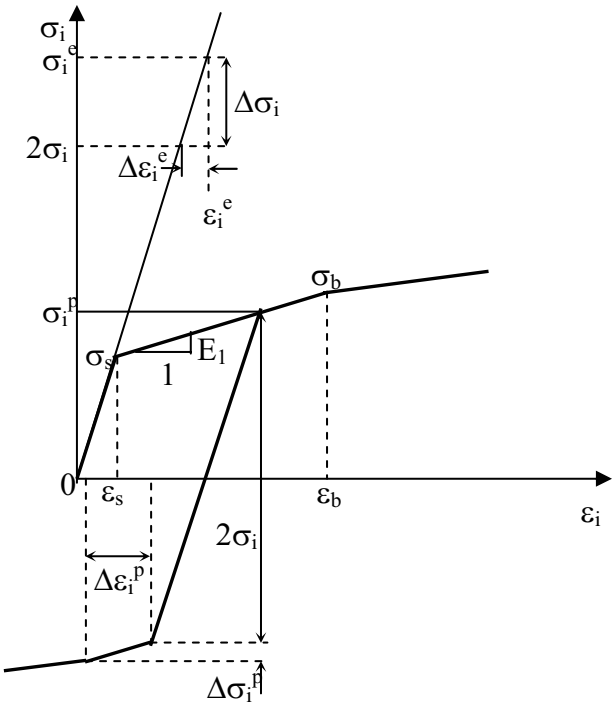

Figure 1 : Schematic diagram for calculating residual stress

4 The residual stress after unloading

Similar to Li, et al. (1991), three assumptions are involved, that are: (a) the deformation is small; (b) unloading is an elastic process before reversed yielding starts; and (c) hydrostatic stresses do not introduce plastic deformation. By means of these assumptions, the basic formula for calculating the residual stress can be written as

$$\sigma_{ij}^r = s_{ij}^p - s_{ij}^e \tag{27}$$

The shot peened material (target material) is assumed to be isotropic. Therefore, the residual stresses can be derived from the following relation:

$$\sigma_{ij}^r = \begin{cases} 0 \text{ for } \sigma_i^e \le \sigma_s \\ s_{ij}^p - s_{ij}^e \text{ for } \sigma_s \le \sigma_i^e < 2\sigma_i^p \end{cases} \tag{28}$$

which illustrates that there is no residual stress in elastic loading stage. Thus, the residual stresses can be expressed as

$$\begin{aligned} \sigma_{11}^r &= \tfrac{1}{3}\left(\sigma_i^p - \sigma_i^e\right) \\ \sigma_{22}^r &= \tfrac{1}{3}\left(\sigma_i^p - \sigma_i^e\right) \text{ for } \sigma_s \le \sigma_i^e \le 2\sigma_i^p \\ \sigma_{33}^r &= -2\sigma_{11}^r \end{aligned} \tag{29}$$

The target material will experience reversed yielding and hardening if $\sigma_i^e \ge 2\sigma_i^p$. Figure 4 shows schematically how to calculate σ^r. A stress of $2\sigma_i^p$ is elastically unloaded first, then reversed yielding take place, but there are still some stresses that have not been unloaded, as shown in figure 4, which can be expressed as

$$\Delta\sigma_i^e = \sigma_i^e - 2\sigma_i^p \tag{30}$$

Now, from the elastic Hook's law and the assumption that the ratio of ε_i^p to ε_i^e on the x_3-axis inside the target is equal to the ratio α of the deformation at the surface, the elastic and elastic-plastic strains corresponding to $\Delta\sigma_i^e$ are obtained, respectively, as

$$\Delta\varepsilon_i^e = \frac{\Delta\sigma_i^e}{E} \tag{31}$$

$$\Delta\varepsilon_i^p = \alpha\Delta\varepsilon_i^e \tag{32}$$

Then, as in Figure 1, the corresponding stress $\Delta\sigma_i^p$ can be obtained by using the multi-linear stress-strain curve.

Thus, the residual stress can be obtained as

$$\begin{aligned}\sigma_{11}^r &= \tfrac{1}{3}\left(\sigma_i^p - 2\sigma_i^p - \Delta\sigma_i^p\right)\\ \sigma_{22}^r &= \tfrac{1}{3}\left(\sigma_i^p - 2\sigma_i^p - \Delta\sigma_i^p\right)\\ \sigma_{33}^r &= -2\sigma_{11}^r\end{aligned} \tag{33}$$

$\sigma^r$is only the residual stress after loading and unloading a single ball. After shot peening with 100% coverage it is assumed that the plastic deformation is steady and continuous. As there is no particular direction on the surface of the semi-infinite body, all the tensors only depended on the depth x_3. The residual stress tensor in the stabilized state is independent of the coordinates (x_1, x_2) and remains constant on any plane parallel to the surface, with $\sigma_{11}^R = \sigma_{22}^R$. The superscript R indicates the residual stress after 100% coverage, i.e. the final residual stress. The boundary conditions on the surface enable us to write:

$$\sigma_{13}^R(0) = \sigma_{23}^R(0) = \sigma_{33}^R(0) = 0$$

The equilibrium equations are reduced to:

$$\frac{\partial\sigma_{13}^R}{\partial x_3} = 0$$

$$\frac{\partial\sigma_{23}^R}{\partial x_3} = 0$$

$$\frac{\partial\sigma_{33}^R}{\partial x_3} = 0$$

So at any depth x_3 we have

$$\sigma_{12}^R(x_3) = \sigma_{13}^R(x_3) = \sigma_{23}^R(x_3) = \sigma_{33}^R(x_3) = 0$$

The equilibrium equations and the boundary conditions for the residual stresses lead to the following residual stress and strain fields

$$\begin{aligned}&\sigma_{11}^R = \sigma_{22}^R = f(x_3),\\ &\sigma_{33}^R = 0\\ &\varepsilon_{11}^R = \varepsilon_{22}^R = 0,\\ &\varepsilon_{33}^R = g(x_3)\end{aligned} \tag{34}$$

It is noted that the stresses (33) fail to satisfy the equilibrium conditions. To obtain the correct residual stress field, equation (33) must be partially relaxed. By means of the Hooke's law, the relaxation values of σ_{11}^r and σ_{22}^r, i.e. $\sigma_{11}^{'}$ and $\sigma_{22}^{'}$, can be obtained as

$$\begin{aligned}\sigma_{11}^{'} &= \tfrac{v}{1-v}\sigma_{33}^r\\ \sigma_{22}^{'} &= \tfrac{v}{1-v}\sigma_{33}^r\end{aligned} \tag{35}$$

Thus, the final residual stressed σ_{11}^R and σ_{22}^R can be obtained as

$$\begin{aligned}\sigma_{11}^R &= \sigma_{11}^r - \tfrac{v}{1-v}\sigma_{33}^r = \tfrac{1+v}{1-v}\sigma_{11}^r\\ \sigma_{22}^R &= \sigma_{22}^r - \tfrac{v}{1-v}\sigma_{33}^r = \tfrac{1+v}{1-v}\sigma_{11}^r\end{aligned} \tag{36}$$

The above procedure is similar to that in reference [Li, et al. (1991)]. However, *it is noted that in reference* [Li, et al. (1991)]*, they assume the shot peening procedure is a static phenomenon; so they did not consider the effect of the velocity. Their model is an empirical relation between the plastic radius a_p of the dent and the equivalent static load F of shot peening which, is extracted by fitting experimental results. The quantity a_p is measured directly from experimental data, and then applied using the empirical relation to evaluate the equivalent static load of shot peening, F. No empirical relations are used in the analyses discussed in this newly developed model, as the quantity a_p is determined by the shot velocity. Therefore, this model is more reasonable, convenient, and simple than that of reference* [Li, et al. (1991)].

It is easy to implement the aforementioned theory to calculate the residual stresses due to shot peening.

5 Verification of the model for shot peening induced residual stresses

We employed this model to simulation the experimental data. The test data include shot-peening residual stress distribution for Al7075-T73, Ti-6Al-4V alpha-beta, and Ti-6Al-4V Beta-STOA. The residual stress measurements have been obtained by the method of *x*-ray diffraction, which is known to have some measure of error. The Al7075-T73 stress distributions include test data for Almen intensities of 0.009N to 0.011N which is a very light shot-peening intensity for aluminum. Also included is measured residual stress data from Metal Improvement for an Almen intensity of 0.016A which is a fairly heavy intensity. Common aluminum shot-peening

Table 1 : Shot Peen Residual Stress

Material	**Intensity**	**Shot Size**
Al7075-T7351	0.009 –0.011N	S170 est.
	0.0016A	S170 est.
Ti-6Al-4V Beta-STOA	0.006 –0.008N	S170 est.
	0.008-0.012A	S170 est.
Ti-6Al-4V Alpha-Beta	0.011A	S170

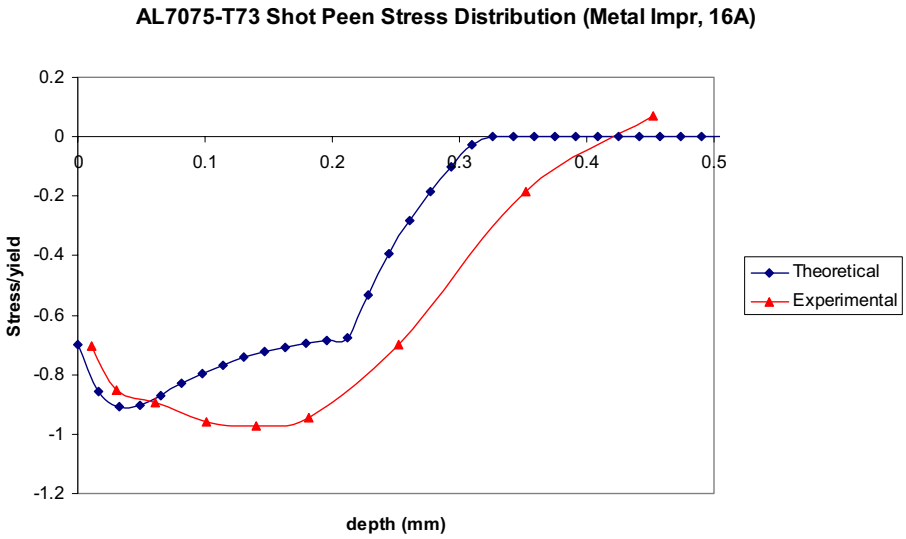

Figure 2 : Comparison of the residual stress for Al7075-T73 Metal Improvement

Almen intensities at the test are around 0.012A. The Ti-6Al-4V Beta-STOA residual stress distributions include test data for Almen intensities of 0.006N to 0.008N, 0.009N to 0.013N, and 0.008A to 0.012A. It is interesting to note that the residual stress distributions for the light (N) intensities and the heavier (A) intensities are similar. The Ti-6Al-4V alpha-beta residual stress distributions include test data for an Almen intensity of 0.011A. The intensity and shot size are shown in Table 1.

For the Al7075-T73 Metal Improvement residual stress data the shot size and velocity are specified. For some test residual stress data these parameters are not provided. This is because it is common practice in the industry to specify the Almen intensity, but not shot size or velocity. The shot size is generally not specified which allows the operator to use any shot size and velocity that achieves the specified Almen intensity. This minimizes the need for the time consuming process of changing the shot in the shot-peening machine. The only restriction on shot size is that the shot size (diameter) must be less than half the radii in the areas being peened. Common shot sizes are S110, S170, and S230. The corresponding nominal diameters are 0.011 inches, 0.017 inches and 0.023 inches, respectively. Virtually all shot-peening at this test has been done with cast steel in conformance with Mil-S-851. In the analysis, we use the following typical values:

Al7075-T73

σ_b = 69 ksi, σ_s = 57 ksi, E =10.5 msi

Ti-6Al-4V Alpha-Beta

σ_b = 145 ksi, σ_s = 135 ksi, E =16.5 msi

Ti-6Al-4V Beta-STOA

σ_b = 150 ksi, σ_s = 140 ksi, E =16.5 msi

Other Typical Properties needed are:

Aluminum: Poison's Ratio=0.33, Density=0.101 lb/in^3, Thickness=0.50 inches, elongation=9%

Titanium: Poison's Ratio=0.33, Density=0.16 lb/in^3, Thickness=0.50 inches, elongation=11%

The Almen intensity is measured using SAE 1070 cold

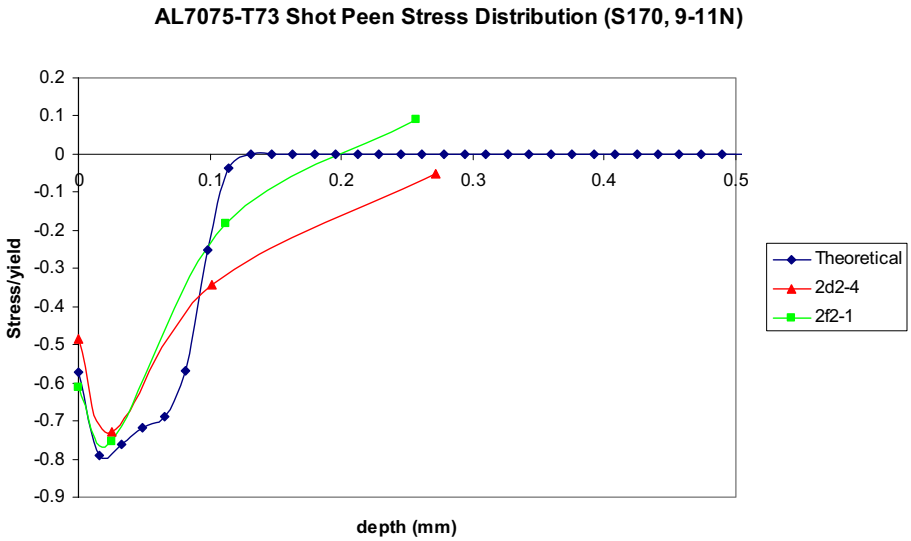

Figure 3 : Comparison of the residual stress for Al7075-T73

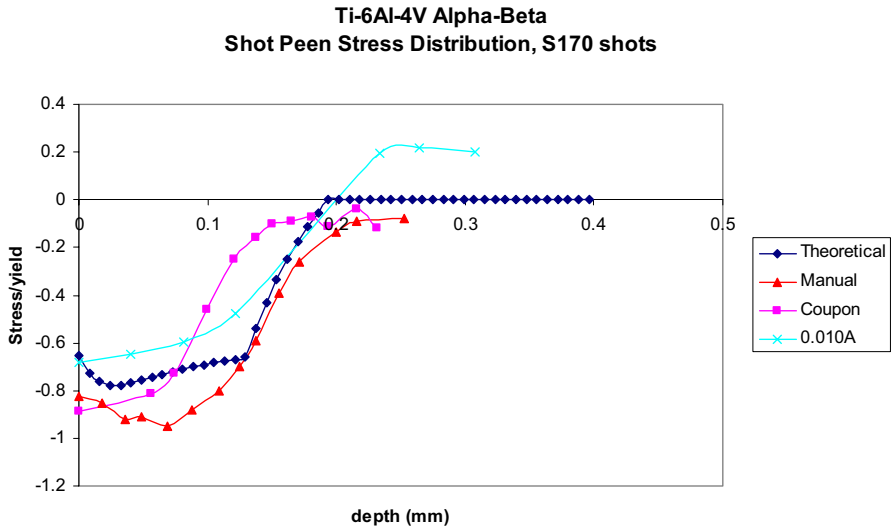

Figure 4 : Comparison of the residual stress for Ti-6Al-4V Alpha-Beta

rolled spring steel strips. These strips measure 3 by 0.75 inches, and when blasted on one side the plastic deformation causes a curvature that is measured on an Almen (dial) gauge. For intensities below 0.004A the type "N" test strip should be used. For comparison of the nominal intensity designations, type "A" test strip deflection may be multiplied by three to obtain the approximate deflection of a type "N" test strip. The relationship between the Almen intensity, shot velocity and shot size can be found in Guagliano (2001). In this paper, we employ this relation to determine the shot velocity. The comparisons of the residual stress distribution from our theoretical model with the experimental data from test are depicted in Figures 2-7. In Fig. 3, there are 2 sets of experiment data: 2d2-4 and 2f2-1. In Fig. 4, there are 3 sets of experiment data: Manual, Coupon and 0.010A, where the "0.010A" means the Almen intensity for this set of experiment results is 0.010A, however, the other sets of experiment data and the numerical result are for Almen intensity 0.011A.

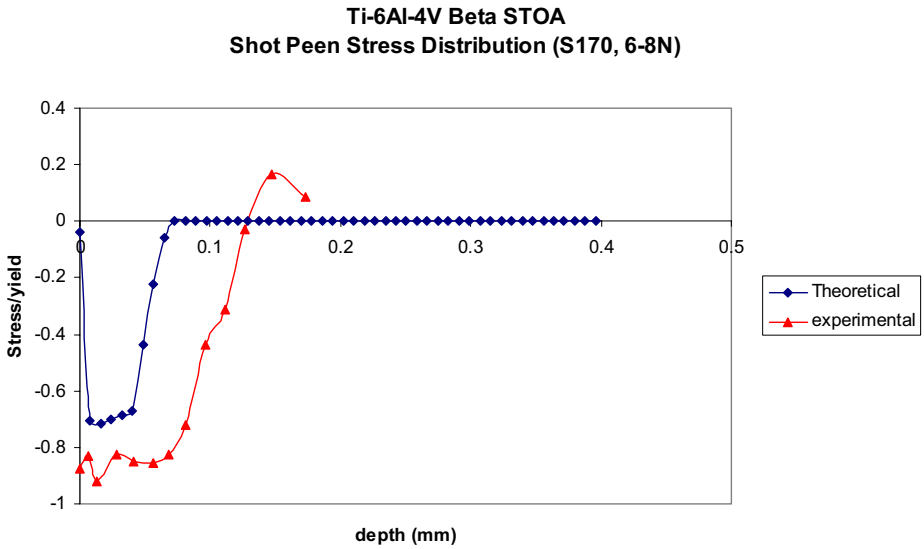

Figure 5 : Comparison of the residual stress for Ti-6Al-4V Beta STOA

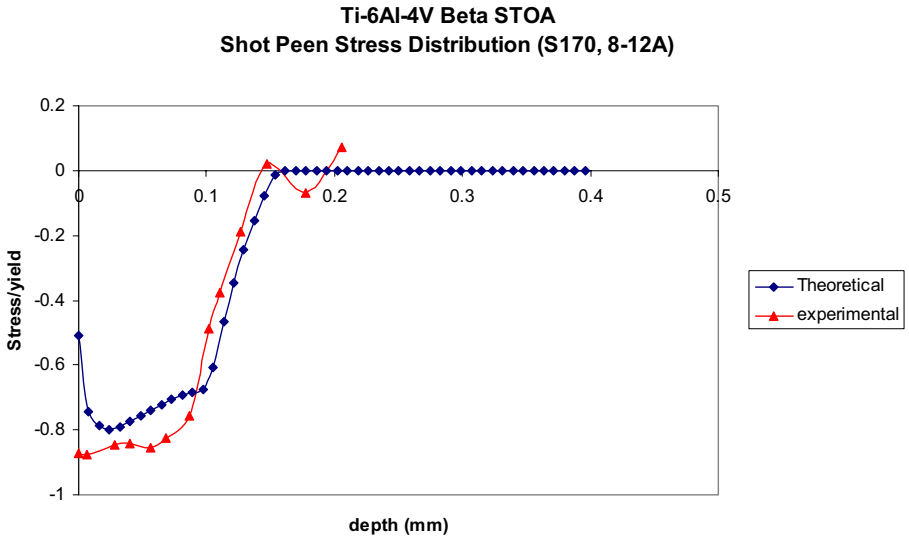

Figure 6 : Comparison of the residual stress for Ti-6Al-4V Beta STOA

From these figures, we can find that the theoretical mode can simulate the experimental results very well. It is also can be found that the high velocity of the sphere will produce a large compressive residual stress zone, and the maximum value of the compressive residual stress increases, as does the velocity of the sphere. However, the simulation results for Ti-6Al-4V Alpha-Beta are somewhat different with the experiment data for 6-8N (Fig. 5) and 9-13N (Fig. 7). The experiment results for the light (N) intensities and the heavier (A) intensities are similar, which is unreasonable.

In the present model, no empirical relation is used, and the quantity a_p is determined by the shot velocity. Very few numerical computations are needed when a classical numerical computation would have been nearly impossible. So, the analysis model appears to be a very suitable tool for industrial purposes. These numerical results were instrumental in concluding that the newly developed analysis model is:

- very simple and quick;

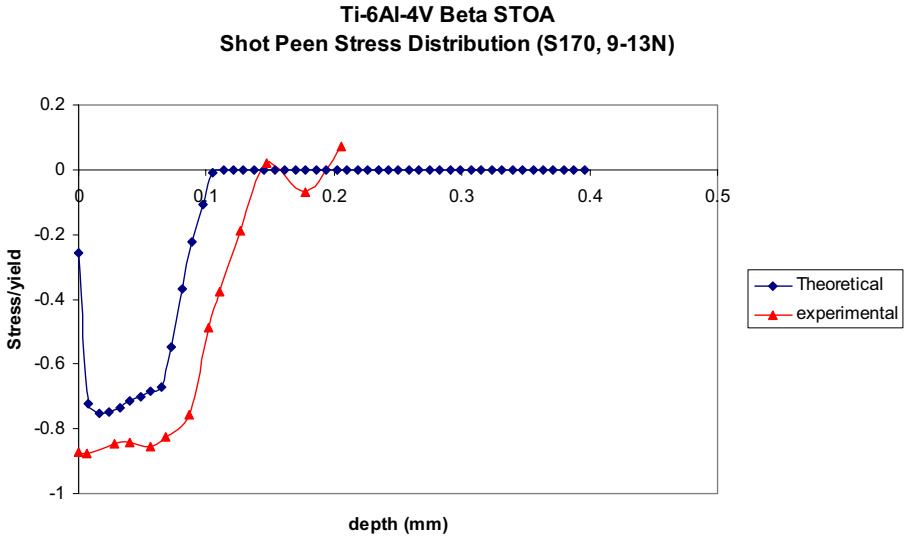

Figure 7 : Comparison of the residual stress for Ti-6Al-4V Beta STOA

- effects of velocity of the shot, diameter of the shot, and the materials characteristics are considered;
- the material can be strain-hardening;
- no empirical parameters are used.

The analysis model can be generalized to arbitrary coverage and finite-thickness work-piece. It should be pointed out that the current model couldn't give the tensile residual stress field that is partly due to the assumption that the target material is semi-infinite. The tensile residual stress field would appear, for finite-thickness target material, as a result of the reflection of the stress waves. The tensile residual stress in finite-size (finite thickness as well as finite in-plane dimensions) specimens, can be introduced by considering that the sum (integration) of residual stresses along the x_3-axis should be zero.

6 Conclusions

The analytical model that is developed in this paper for shot peening is promising. The results of validation of this model for predicting residual stress field, against the test data, are very good. Within reasonable accuracy, the experimentally observed effects were found in the present analytical model, and very few numerical computations are required. In contrast, a complete numerical computation, such as finite element method (FEM) would have been extremely intensive, computationally inefficient, and entirely unrealistic. Therefore, the present analysis model appears to be a very suitable tool for commercial analyses, although the MLPG method [Sladek, et al. (2004); Han and Atluri (2004a, b); Atluri and Shen (2005); Han, et al. (2005, 2006); Atluri, et al. (2004, 2006a, b); Liu, et al. (2006)] may be another powerful tool.

Acknowledgement: This work was supported by the Federal Aviation Administration, Materials and Structures Branch, AAR-450, located at the William J. Hughes Technical Center, Atlantic City International Airport, New Jersey.

References

Al-Hassani, S. T. S. (1981): Mechanical aspects of residual stress development in shot peening. ICSP1, Paris.

Al-Hassani, S. T. S. (1982): Shot peening mechanics and structures. *SAE* paper, 821452.

Al-Hassani, S. T. S. (1984): An engineering approach to shot peening mechanics. *Proc. Of the second Int. Conf. On Shot Peening*, ICSP-2 (H. O. Fuchs ed.). Paramus, NJ: ASPS, p275.

Atluri, S. N.; Han, Z. D.; Rajendran, A. M. (2004): A New Implementation of the Meshless Finite Volume Method, Through the MLPG "Mixed" Approach. *CMES: Computer Modeling in Engineering & Sciences* 6: 491-514.

Atluri, S. N.; Liu, H. T.; Han, Z. D. (2006a): Mesh-

less Local Petrov-Galerkin (MLPG) Mixed Collocation Method For Elasticity Problems. *CMES: Computer Modeling in Engineering & Sciences* 14: 141-152.

Atluri, S. N.; Liu, H. T.; Han, Z. D. (2006b): Meshless Local Petrov-Galerkin (MLPG) Mixed Finite Difference Method for Solid Mechanics. *CMES: Computer Modeling in Engineering & Sciences* 15: 1-16.

Atluri, S. N.; Shen, S. (2005): MSimulation of a 4^{th} Order ODE: Illustration of Various Primal & Mixed MLPG Methods. *CMES: Computer Modeling in Engineering & Sciences* 7: 241-268.

Davis, R. M. (1948): The determination of static and dynamic yield stresses using a steel ball. *Proc. Roc. Soc. A* 197: 416.

Deslaef, D.; Rouhaud, E.; and Rasouli-Yazdi, S. (2000): 3D finite element models for shot peening processes. *Materials Science Forum* 347-349: 241-246.

Guagliano, M. (2001): Relating Almen intensity to residual stresses induced by shot peening: a numerical approach. *Journal of Materials Porcessing Technology* 110: 277-286.

Guechichi, H.; Castex, L.; Frelat, L.; Inglebert, G. (1986): Predicting residual stress due to shot peening. *Impact surface treatment*, (S.A.. Meguid edited), Elsevier, Applied Science Publishers LTD.

Han, Z. D.; Atluri, S. N. (2004a): Meshless Local Petrov-Galerkin (MLPG) approaches for solving 3D Problems in elasto-statics. *CMES: Computer Modeling in Engineering & Sciences* 6: 169-188.

Han, Z. D.; Atluri, S. N. (2004b): A Meshless Local Petrov-Galerkin (MLPG) Approach for 3-Dimensional Elasto-dynamics. *CMC: Computers, Materials & Continua* 1: 129-140.

Han, Z. D.; Rajendran, A. M.; Atluri, S. N. (2005): Meshless Local Petrov-Galerkin (MLPG) Approaches for Solving Nonlinear Problems with Large Deformations and Rotations. *CMES: Computer Modeling in Engineering & Sciences* 10: 1-12.

Han, Z. D.; Liu, H. T.; Rajendran, A. M.; Atluri, S. N. (2006): The Applications of Meshless Local Petrov-Galerkin (MLPG) Approaches in High-Speed Impact, Penetration and Perforation Problems. *CMES: Computer Modeling in Engineering & Sciences* 14: 119-128.

Johnson, K. L. (1986): *Contact Mechanics*, Cambridge University Press.

Khabou, M. T.; Castex, L.; and Inglebert, G. (1990): The effect of material behavior law on the theoretical shot peening results. *Eur. J. Mech., A/Solids* 9: 537-549.

Li, J.K.; Yao, M.; Wang, D.; and Wang, R. (1991): Mechanical approach to the residual stress field induced by shot peening. *Materials Sci. and Engineering* A 147: 167-173.

Liu, H. T.; Han, Z. D.; Rajendran, A. M.; Atluri, S. N. (2006): Computational Modeling of Impact Response with the RG Damage Model and the Meshless Local Petrov-Galerkin (MLPG) Approaches. *CMC: Computers, Materials & Continua* 4: 43-54.

Meguid, S. A.; Shagal, G.; Stranart, J. C. (1999): Finite element modeling of the shot-peening residual stresses. *Journal of Materials Processing Technology* 92-93: 401-404.

Schiffner, K.; Helling, C.D.G. (1999): Simulation of residual stresses by shot peening. *Computers and Structures* 72: 329-340.

Sladek, J.; Sladek, V.; Atluri, S. N. (2004): Meshless Local Petrov-Galerkin Method in Anisotropic Elasticity. *CMES: Computer Modeling in Engineering & Sciences* 6: 477-490.